Energy Conversion and Management 302 (2024) 118095

Contents lists available at ScienceDirect

Energy Conversion and Management

journal homepage: www.elsevier.com/locate/enconman

Synergistic effects of the mixing factor on the kinetics and products obtained by co-pyrolysis of *Rosa rubiginosa* rosehip seed and husk wastes

Rodrigo Torres-Sciancalepore [a], Daniela Nassini [b], Daniela Asensio [a], Ana Bohé [c], Rosa Rodriguez [d], Gastón Fouga [c], Germán Mazza [a,*]

[a] Instituto de Investigación y Desarrollo en Ingeniería de Procesos, Biotecnología y Energías Alternativas, PROBIEN (CONICET-Universidad Nacional del Comahue), Calle Buenos Aires 1400, Neuquén 8300, Argentina
[b] Departamento de Fisicoquímica y Control de Calidad, Complejo Tecnológico Pilcaniyeu, Centro Atómico Bariloche, Comisión Nacional de Energía Atómica (CNEA), Av. Bustillo 9500, S.C. de Bariloche 8400, Argentina
[c] Departamento de Fisicoquímica y Control de Calidad, Complejo Tecnológico Pilcaniyeu, Centro Atómico Bariloche, Comisión Nacional de Energía Atómica and Consejo Nacional de Investigaciones Científicas y Técnicas (CONICET), Av. Bustillo 9500, S.C. de Bariloche 8400, Argentina
[d] Instituto de Ingeniería Química - Facultad de Ingeniería, Universidad Nacional de San Juan - Grupo Vinculado al PROBIEN (CONICET-UNCo), Av. Libertador San Martín (Oeste) 1109, San Juan 5400, Argentina

ARTICLE INFO

Keywords:
Slow pyrolysis
Co-pyrolysis
Rosehip waste
Synergistic effects
Biomass blend
Kinetic parameters

ABSTRACT

The aim of this work was to study the potential synergistic effects of the mixing factor on the kinetics parameters and products obtained through co-pyrolysis of two wastes from *Rosa rubiginosa* rosehip, and further co-gasification with CO_2 of the remaining biochar. Thermogravimetric analysis showed that 6 different processes occur by slow pyrolysis (heating rates of 5, 10, and 20 °C/min), associated with the decomposition of hemicelluloses, cellulose, lignin, and $CaCO_3$ from the ashes. Isoconversional methods determined activation energies of 84.68–223.42, 230.11–270.85, 187.58–303.37, and 400.11–421.71 kJ/mol for hemicellulose, cellulose, lignin, and $CaCO_3$ decomposition, respectively. In most cases, the activation energy from co-pyrolysis was higher for the blends than for the pure wastes, which means that the blends are less reactive to pyrolysis. Gas and tar analyses showed that the blend with 75 % husk waste and 25 % seed waste produced the most hydrogen (5.639 mmol/g biomass), while the blend with 25 % husk waste and 75 % seed waste produced the most carbon monoxide (3.642 mmol/g biomass). The biochar produced by the blends and pure wastes were thermally treated with CO_2 to compare reactivity to gasification. It was concluded that the addition of husk waste to the blend increases the reactivity of the biochar obtained, mainly due to its higher ash content.

1. Introduction

Rosa rubiginosa, a shrub native to Europe and Asia, grows in southern Argentina, Chile, Australia and New Zealand [1]. Its ready adaptation to a wide range of soils [1,2] endows it with colonizing characteristics, enabling it to push other plants and animals to extinction [3]. In Argentina, *Rosa rubiginosa* and other *Rosaceae* species are considered invasive [3–5], though it is still permitted to use rosehips for economic purposes. In Argentina and Chile, the main rosehip market is for rosehip oil, flour from the seed, and jam from the husk [6]. Research has shown that *Rosa rubiginosa* seed oil has skin healing properties, especially for the treatment of scars, burns [7,8], and diabetic skin wounds [9]. Some preliminary studies have shown that it could help prevent hepatic steatosis (fatty liver) [10].

Rosehip seed and husk processing produces different residues that must be taken into consideration. Circular bioeconomy and the development of biorefinery technologies aim to process biomass into multiple products and energy, leaving no residue [11]. These products include fuels, feed, biopolymers, and biopharmaceuticals, among others [12]. It is therefore possible, through this biorefinery approach, not only to reduce pollution by treating the waste left in the process, but also to mitigate the effect of the increasing demand for energy and materials.

Pyrolysis and gasification are two thermochemical processes through which it is possible both to valorize biomass wastes and obtain biogas such as hydrogen, carbon monoxide, methane, and ethylene, among others. Pyrolysis can also be used to produce bio-oil and biochar [13].

* Corresponding author.
E-mail address: german.mazza@probien.gob.ar (G. Mazza).

https://doi.org/10.1016/j.enconman.2024.118095
Received 17 November 2023; Received in revised form 27 December 2023; Accepted 11 January 2024

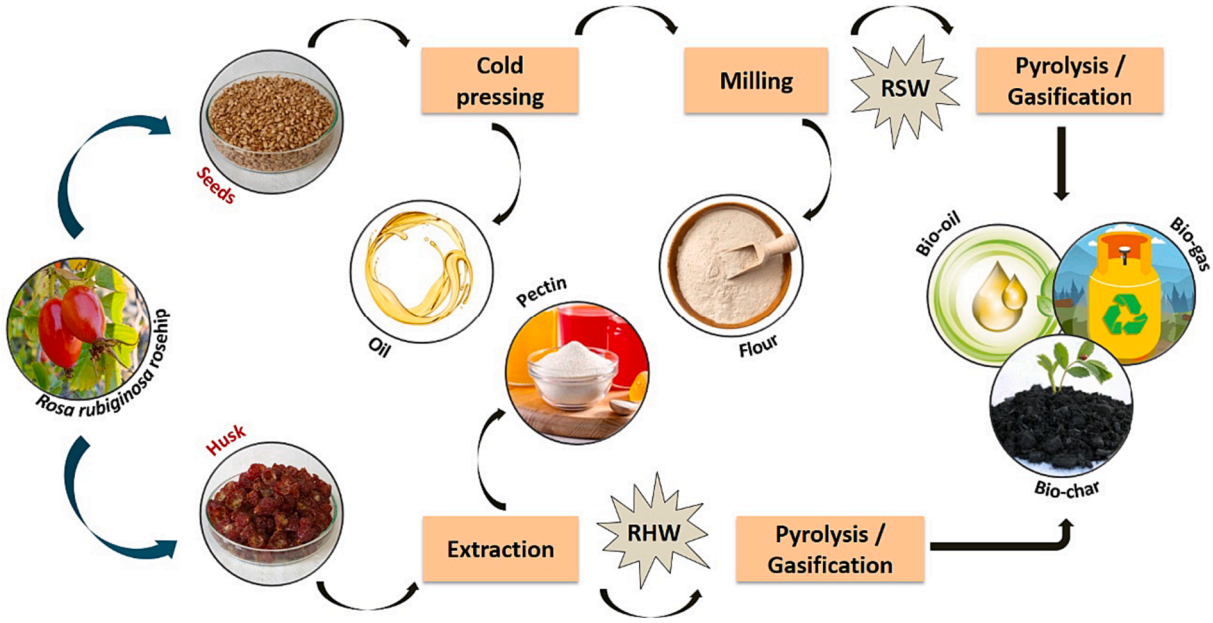

Fig. 1. Diagram of rosehip processing up to final waste (RHW and RSW). The current study focuses on the pyrolysis/gasification process in the diagram.

The bio-oil may be burned for energy or distilled to obtain multiple products. Biochar is a well-known adsorbent for cleaning gas [14,15], and can also be used to remediate soils [16,17]. Among the most recently published research, Mu et al. [18] performed a comparative study on the pyrolysis of crop, woody, and herbaceous biomass to assess the products and the characteristics of the biochar and its response to CO_2 gasification. Ahmed and Kishore [19] studied the extraction of the fuel phase from bio-oil obtained by slow pyrolysis of *Azadirachta indica* biomass. Wu et al. [20] analyzed the effects of the interaction of the components in lignocellulosic biomass (hemicellulose, cellulose and lignin) on the pyrolysis products and kinetics. Chen et al. [21] reviewed the advances in co-pyrolysis of biomass with carbonaceous materials (plastic wastes, tire garbage, coal, etc.) and its synergistic effects. Other recent research focuses on the analysis of integrated pyrolysis models by performing simulations in Aspen Plus [22,23].

These processes are conducted in pyrolyzers and gasifiers. Their design and optimization, as well as computer simulations, require the conduction of prior experiments to identify the products obtained and the kinetics of the process. Testing includes thermogravimetry (TGA) and different analytical methods such as Fourier-transform infrared spectroscopy (FTIR), gas chromatography (GC), or mass spectroscopy (MS). Several authors have successfully used thermogravimetric data to identify the kinetic parameters from the Arrhenius model (activation energy, E, and pre-exponential factor, A) and the reaction model [24,25]. Mishra et al. [26] conducted a comparative study on the pyrolysis kinetics of little millet and sunflower stems biomass through thermogravimetric analysis using isoconversional methods, concluding that both biomasses are suitable for this type of process. Sharma et al. [27] compared the pyrolysis of two biomasses (poplar and eucalyptus wood) using model-fitting methods. In both these studies, master plots were used to obtain the kinetic model. Other researchers conducted kinetic studies through multi-step reaction models, by isolating different reactions through deconvolution of the thermogravimetric data [28,29].

The aim of the current study is to use pyrolysis and gasification to analyze potential valorization of rosehip waste from different processes, framed in a biorefinery approach. Two different wastes were studied: rosehip husk waste (RHW) and rosehip seed waste (RSW), both of which are solids remaining after rosehip is subjected to different processes to obtain multiple products, as shown in Fig. 1.

Rosehip seeds are cold pressed and milled in Bariloche, Argentina by *Flores Norpatagonicas S.R.L.*, which sells both the oil and the flour. A previous study by Torres-Sciancalepore et al. [29] discusses the optimization of the pectin extraction from rosehip husk. As shown in Fig. 1, by valorizing the remaining residues, it is possible to close the loop, leaving *zero waste* and obtaining multiple products. This way, a company dedicated to the processing of the rosehip from *Rosa rubiginosa* will be able to obtain multiple products, including the pyrolyzer/gasifier in one place avoiding additional transportation costs.

Furthermore, special attention was put into identifying potential synergistic effects produced by the mixing factor on different blends of the two wastes. These effects can either potentiate or inhibit the production of certain substances, or cause unexpected changes in the kinetic parameters. Knowledge of these effects will contribute to improved decision-making regarding process design.

2. Materials and methods

2.1. Materials

Two wastes from *Rosa rubiginosa* rosehip were treated in this study: rosehip seed waste (RSW) and rosehip husk waste (RHW). RSW was provided by *Flores Norpatagónicas S.R.L.*, a company that produces seed oil for cosmetics (by cold pressing without chemical additives), and rosehip seed flour. RHW is the exhausted solid remaining after pectin extraction with citric acid at pH = 2.3 and T = 79.6 °C [29]. Both wastes were dried at 70 °C for 24 h in a free convection oven (San Jor SL30SDB). Samples were shredded and stored separately in airtight bags until further use.

Three blends were prepared by mixing the two residues in different mass ratios, RHW:RSW = 1:3, 1:1, and 3:1, which were labeled RHW25, RHW50, and RHW75, respectively. The pure RSW sample was labeled RHW0, and the pure RHW sample RHW100.

2.2. Characterization of rosehip wastes

Ash content (ASH) by proximate analysis, volatile matter (VM) and fixed carbon (FC) contents were determined for all samples, following standards ASTM E 871-82, ASTM E 872-82, and ASTM D 1102-84 for determining moisture content, VM and ASH respectively, while FC was calculated by difference.

2.3. Pyrolysis experiments

2.3.1. Thermogravimetry

To acquire data on biomass decomposition by pyrolysis with time and temperature, thermogravimetric experiments were performed on all samples in a thermobalance, thermal analyzer NETZSCH STA 409. A 40 mg sample was placed in a crucible in the thermal analyzer and heated from ambient temperature to 950 °C at heating rates (β) of 5, 10 and 20 °C/min. The pyrolysis experiments in the thermobalance were performed in an inert atmosphere using a 5 L/h nitrogen gas (N_2) flow rate. To study the effect of the blends, the DTG (derivative thermogravimetric) curve was constructed by numerical differentiation of data using a second-order Lagrange interpolating polynomial.

2.3.2. Determination of kinetic and thermodynamic parameters

Based on the thermogravimetric data, dα/dT plots were constructed, where α is the degree of conversion with respect to the total devolatilization of the sample at the end of the pyrolysis process ($\alpha = (m_0 - m)/(m_0 - m_\infty)$). The new plots were therefore deconvoluted and different peaks were isolated and adjusted with the Lorentz function [30], which showed the best fit among several distribution models that were tested. Each peak represented a different disintegration reaction and was attributed to the decomposition of different pseudocomponents that constituted the biomass. From each isolated process, the kinetic parameters, pre-exponential factor (A), activation energy (E), and conversion model (f(α), were determined following the Arrhenius equation within the reaction rate:

$$\frac{d\alpha}{dT} = \frac{A}{\beta}\exp\left(-\frac{E}{RT}\right)f(\alpha) \quad (1)$$

following the methodology reported by Torres-Sciancalepore et al. [30].

The activation energy for each reaction was determined by isoconversional methods, from which the Fynn-Wall-Ozawa (FWO), Kissinger-Akahira-Sunose (KAS) and Starink were tested [25,30–32]. The coefficient of determination (R^2), the mean squared error (MSE) and the absolute average deviation (AAD) were assessed as criteria for selecting the method that fitted the best.

The method to determine the pre-exponential factor, A, was based on the kinetic compensation effect (KCE) [25,30,33,34]. The KCE is a model-fitting method in which several conversion models, f(α), are used to find the compensation parameters *a* and *b* from the following equation:

$$\ln A = a + b\,E \quad (2)$$

The definition of each model used is presented in the Supplementary Material, Table S1.

Finally, the master plots method was selected to determine the fitting conversion model, f(α), from the list in Table S1 of the Supplementary Material [25,30,35,36]. The method consisted of finding the theoretical function $g(\alpha) = \int_0^\alpha d\alpha/f(\alpha)$ that best fitted the experimental results P(E/RT) in the following equation:

$$\frac{g(\alpha)}{g(\alpha = 0.5)} = \frac{P\left(\frac{E}{RT(\alpha)}\right)}{P\left(\frac{E}{RT(\alpha=0.5)}\right)} \quad (3)$$

where $P(E/RT) = 0.0048\exp(-1.0516E/RT)$ is Doyle's approximation and it is a function of conversion. The coefficient of determination was calculated to determine which of the models fitted best.

To estimate the activation enthalpy and activation Gibbs energy, the following equations were used [35]:

$$\Delta H = E - RT_m \quad (4)$$

$$\Delta G = E + RT_m \ln(k_B T_m/hA) \quad (5)$$

where T_m is the maximum decomposition rate temperature (K), k_B is the Boltzmann constant (1.381×10^{-23} J/K), and h is Planck's constant (6.626×10^{-34} J s).

2.3.3. Pyrolysis reactor

Pyrolysis experiments were conducted in a 70-cm-long cylindrical pyrolysis reactor constructed of silica glass to analyze the gases (GC/FTIR), the tar (GC–MS) and the char (SEM) obtained (See Sections 2.3.3.1–2.3.3.3).

For each sample, a crucible containing exactly 50.0 mg of biomass was placed inside the horizontal reactor, which was heated from ambient to 950 °C using an electric furnace with a Dhacel CD101 temperature controller at a heating rate of 5 °C/min in an inert atmosphere using a nitrogen gas (N_2) flow of 5 L/h.

To determine the gas, liquid and solid yields, the pyrolysis reactions were replicated (N_2 flow rate = 5 L/h; T = 950 °C; β = 5 °C/min) in a vertical silica-glass reactor packed with alumina beads. The reactor containing the sample inside the crucible and the ceramic beads was weighed before and after the reactions took place. The liquid fraction condensed on the surface of the beads with the aid of a cooling coil that was in contact with the walls of the reactor and placed far from the heating point, which allowed only the non-condensable gases to escape from the reactor. The gas yield was obtained by difference and the liquid yield was calculated after subtracting the biochar yield (determined by weighing the crucible) as shown in the following equations:

$$\eta_{gas} = \frac{\text{mass of reactor with sample before pyrolysis} - \text{mass of reactor with sample after pyrolysis}}{\text{original sample mass}} \times 100 \quad (6)$$

$$\eta_{biochar} = \frac{\text{sample mass after pyrolysis}}{\text{original sample mass}} \times 100 \quad (7)$$

$$\eta_{liquid} = 100 - \eta_{biochar} - \eta_{gas} \quad (8)$$

2.3.3.1. Gaseous pyrolysis products: GC/FTIR. The horizontal tubular reactor described in Section 2.3.3 was connected online with a Perkin Elmer Spectrum 400 FTIR spectrometer to detect the non-condensable gases. The connected cell inside the spectrometer had two NaCl windows. Absorbance spectra (wavenumber 4000 cm^{-1} to 625 cm^{-1}) were recorded every 10 °C (2 min).

Hydrogen gas (H_2) in the non-condensable pyrolysis products was detected with a Gas Chromatograph SRI Instrument Model 8610C with a thermal conductivity detector (TCD). Small samples of the gas were extracted with a 1 mL syringe and injected into a chromatographic column (Alltech Column CTR I (1.82 m × 0.63 cm)) at 50 °C with argon at a 2 mL/min flow rate.

2.3.3.2. Condensable pyrolysis products (bio-oil): GC–MS. The volatiles that condensed inside the horizontal reactor were collected and dissolved in HPLC-grade acetone to a concentration of 2 mg tar/ml acetone.

The solution was injected at 250 °C into a gas chromatograph (Perkin Elmer Clarus 680, chromatographic column: Elite-5MS) with a mass spectrometer (Perkin Elmer Clarus 600 T) (GC–MS). A flow rate of 1 mL/min of helium was used as carrier gas. The oven was heated at a rate of 3 °C/min to a temperature of 235 °C, which was maintained for 13 min, with a total analysis time of 80.33 min. Data were acquired with the software TurboMass Version 5.4.2.1617, 2008 (Perkin Elmer), and the separated compounds in the column were identified with NIST/EPA/NIH Mass Spectral Library (version 2.0f) using the software NIST Mass Spectral Search.

2.3.3.3. Solid pyrolysis products (biochar): SEM-EDS. The solid carbon product remaining in the crucible after pyrolysis, known as biochar, was collected from the horizontal reactor and analyzed with a FIB-SEM Carl ZEISS Crossbeam 340 scanning electron microscope with energy dispersive spectroscopy (SEM-EDS). The biochar obtained from each sample was subsequently submitted to gasification with CO_2 to compare reactivity (see Section 2.4).

2.4. CO_2 gasification of the biochar

The biochar obtained was submitted to gasification with CO_2 both in a thermobalance and in the horizontal silica glass reactor described in Sections 2.3.1 and 2.3.3. Previous tests were performed with different CO_2 flow rates and different sample masses until no changes were observed in the gasification thermograms to avoid any mass transfer restriction. Finally, the gasification was carried out with a CO_2 flow rate of 1 L/h to a biochar mass sample of 2.0 mg. The heating rate used to perform the gasification was 5 °C/min in order to allow the FTIR spectrometer to obtain the spectra every 5 °C.

2.5. Numeric synergistic effect (SE) calculation

When two or more different feedstocks are mixed and subjected to thermochemical processes together, it might be possible to observe effects that are different from expected. These differences between the experimental results and the theoretical ones are due to synergy. The synergistic effects, which represent the relative difference between the theoretical and the actual experimental results, may be calculated as follows [37]:

$$SE(\xi) = \left(\frac{\text{Experimental value of } \xi \; - \; \text{theoretical value of } \xi}{\text{theoretical value of } \xi}\right) \times 100\% \qquad (9)$$

where ξ is the parameter or property analyzed or calculated, such as proximate composition, yield or the activation energy from a certain reaction.

The theoretical value for the binary blends in this work is calculated as follows [37]:

$$\text{Theoretical value of } \xi \; = w_{RHW}\xi_{RHW} + w_{RSW}\xi_{RSW} \qquad (10)$$

where w_{RHW} and w_{RSW} are the mass fractions of RHW and RSW respectively, and ξ_{RHW} and ξ_{RSW} are the measured property, characteristic or parameter in the experiment of pure RHW and RSW respectively.

A positive SE means that the observed result is higher than expected by theoretical calculation, while a negative SE means that the observed result is lower than expected by theoretical calculation.

3. Results and discussion

3.1. Biomass characterization results

High volatile matter (VM) content is desirable for producing bio-oil, while higher fixed carbon (FC) content is desirable for producing biochar [38]. As shown in Fig. 2, there are synergistic effects in all blends. For instance, FC for blend RHW25 was higher than expected theoretically, making it the best blend selection for pyrolysis if the aim is to produce biochar. As may be observed in Fig. 2, the blends RHW25 and RHW50 reached SE(FC) higher than 20%. Moreover, RHW25 still produced a small amount of ash compared to pure RHW, which is desirable for obtaining low-ash biochar. On the contrary, to produce bio-oil, it would probably be preferable to process pure RSW or RHW, since all blends presented a negative SE(VM). Regarding the ash content, the blends showed no synergistic effects, with ASH rising with the increase in RHW content.

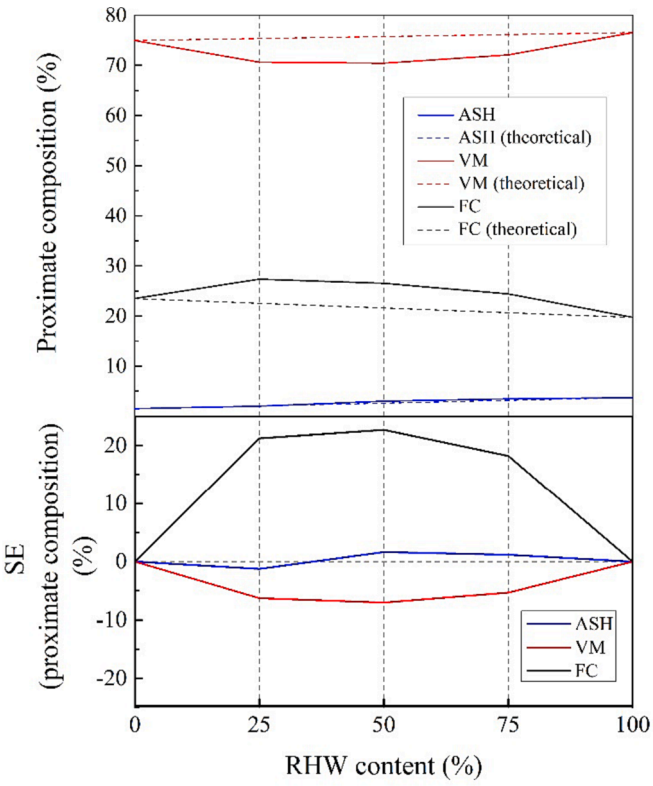

Fig. 2. Proximate analysis expressed on a dry basis for RSW (RHW0), RHW (RHW100) and each blend (RHW25, RHW50, and RHW75).

For RHW, RSW and the blends, VM was 70% to 75%, FC was 23% to 27%, and ASH was 1.5% to 4%. These values are similar to other biomasses reported in the literature [38,39].

Synergistic effects, like the ones observed in Fig. 2, can have multiple origins since they are the result of physicochemical interactions in a microscope scale between the two wastes in the blend. However, some authors have hypothesized that the ash within one waste can have catalytic or inhibitor effects on the other biomass producing different effects [37,40,41]. The presence of RHW ashes may be responsible for the decrease in the volatiles released in the blends (with the corresponding increase in the fixed carbon proportion). These ashes might inhibit the production of volatile compounds while increasing the biochar (FC + ASH) yield.

Contrary to the positive SE observed for FC, Salema et al. [42] studied the co-pyrolysis of oil palm biomass and sawdust and found that the blends produced less biochar (FC + ASH) than the pure blends. The same happened in the co-pyrolysis of rice husk and bamboo dust with sawdust studied by Mallick et al. [43] showing a biochar yield lower than expected.

Ultimate analysis and HHV/LHV results of these pure wastes were previously published by Torres-Sciancalepore et al. [29,30], and are available in the Supplementary Material, Table S2.

3.2. Thermogravimetric and kinetic analyses

The thermogravimetric data collection was numerically differentiated to construct the curve presented in Fig. 3 (DTG), which shows the dm/dT results of RHW(0–100) pyrolysis. The six different peaks observed in Fig. 3, indicated from R1 to R6, are associated with different decomposition steps or reactions that occur in the pyrolysis process. The peak at around 100 °C was not particularly identified with a number because it represents the evaporation step of the remaining moisture. Reactions R1 and R2 (with a peak at 200 °C and 235 °C, respectively) are characteristic of RHW100 pyrolysis, since they are not observed in RHW0. On the contrary, the reaction R3 (with a peak at 280 °C) is present in RHW0 but not in RHW100. These reaction R1–R3 are most likely related to the decomposition of hemicelluloses, given the temperature intervals at which they appear [44,45]. The differences in peak temperatures (between RHW0 and RHW100) might be a consequence of the different components of the biomass wastes, or a response to the different pre-treatments these wastes undergo. Seed waste, RHW0, was not subjected to any chemical process, leaving the hemicellulose chains practically intact, whereas husk waste, RHW100, was pre-treated with citric acid, a weak acid that may cause partial hydrolysis of the polymeric chains in hemicelluloses. The hydrolysis products left may be more susceptible to pyrolysis, leading to a shift of the peaks observed in the DTG curve towards lower temperatures. This was previously described by Torres-Sciancalepore et al. [46].

Alternatively, the separation of peaks in the case of hemicelluloses decomposition has been previously detected by other authors studying the decomposition of xylan, a major constituent of plant hemicelluloses [44,47,48]. Sanchez-Silva et al. [48] suggest that the presence of two peaks for the decomposition of xylan is related to the decomposition of the xylan side units and the cracking of the main xylan chains. In the case of the blends co-pyrolysis, the behavior was as expected, showing intermediate decomposition rates of the components according to the mass proportion of each waste. Thus, the amplitudes of peaks representing R1–R3 for the blends (RHW25, RHW50 and RHW75) were in between those of the pure wastes (RHW0 and RHW100).

The narrow peak with high amplitude located at around 340 °C (Corresponding to reaction R4), is characteristic of cellulose decomposition [45,49]. It was more prominent in RHW0 pyrolysis and decreased with the addition of husk waste, meaning that the seed waste contained a greater proportion of cellulose than the husk waste.

Lignin is also one of the major components of lignocellulosic biomass. Its decomposition by pyrolysis occurs at a wider range of temperatures than the other components mentioned, and typically, its maximum decomposition rate is at approximately 400 °C [50]. Fig. 3 shows a broad peak with a maximum near 400 °C, representing the reaction R5, related to the pyrolysis reactions of lignin. The amplitude of the R5 peak for each sample suggests that husk waste, RHW100, has a higher proportion of lignin than seed waste, RHW0.

The peak at around 690 °C corresponding to the reaction R6 has the greatest amplitude for RHW100 and is barely noticeable for the other samples. This reaction is highly likely to be related to $CaCO_3$ decomposition into CO_2 and CaO, as discussed by Torres-Sciancaleopore et al. [29].

To sum up, the model of parallel reactions considered in this study is as follows:

$$\text{R1}: \text{Hemicelulose}_1 \rightarrow \text{gas} + \text{tar} + \text{biochar} \quad (11)$$

$$\text{R2}: \text{Hemicelulose}_2 \rightarrow \text{gas} + \text{tar} + \text{biochar} \quad (12)$$

$$\text{R3}: \text{Hemicelulose}_3 \rightarrow \text{gas} + \text{tar} + \text{biochar} \quad (13)$$

$$\text{R4}: \text{Cellulose} \rightarrow \text{gas} + \text{tar} + \text{biochar} \quad (14)$$

$$\text{R5}: \text{Lignin} \rightarrow \text{gas} + \text{tar} + \text{biochar} \quad (15)$$

$$\text{R6}: CaCO_3 \rightarrow CaO + CO_2 \quad (16)$$

The complete thermograms TG/DTG at $\beta = 5$, 10 and 20 °C/min are provided in Figs. S1–S5 in the Supplementary Material.

Fig. 4 shows the results of the kinetic and thermodynamic study with the temperature of maximum decomposition rate (T_m), activation

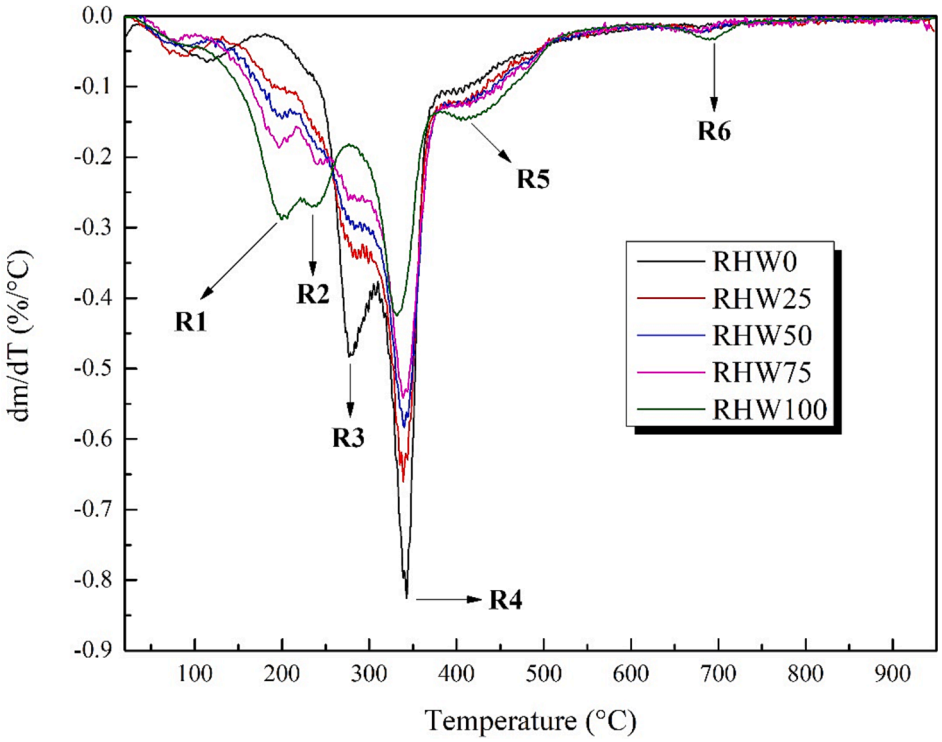

Fig. 3. Derivative thermogravimetric curve (DTG) (for $\beta = 5$ °C/min): decomposition rate of RSW (RHW0), RHW (RHW100) and each blend (RHW25, RHW50, and RHW75). RSW and RHW curves are adapted from Torres-Sciancalepore et al. [29,30].

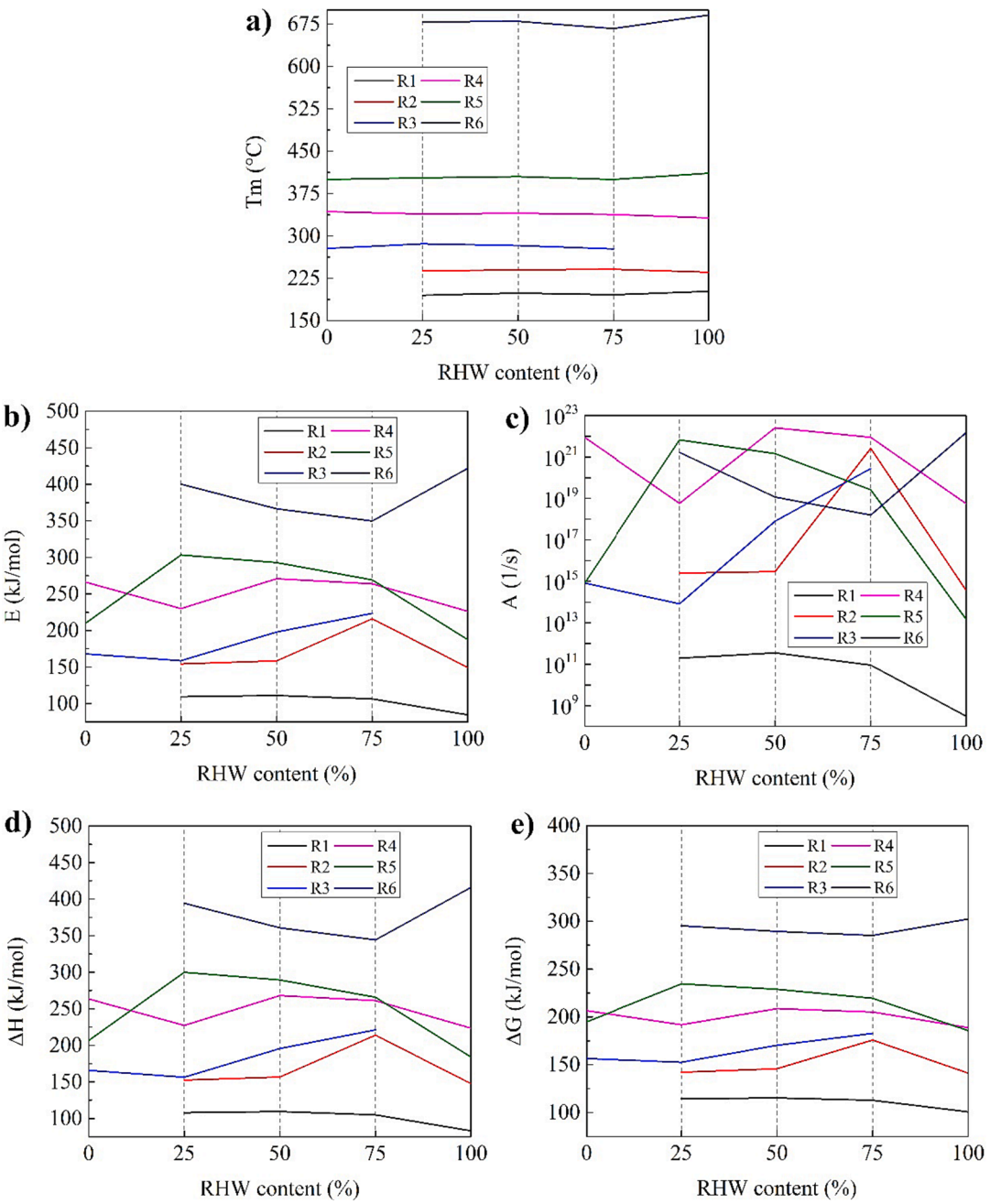

Fig. 4. Graphic results of (a) the temperature of maximum decomposition rate, (b) the activation energy, (c) the pre-exponential factor, (d) the activation enthalpy and, (e) the activation free Gibbs energy. The results of pure wastes were previously published by Torres-Sciancalepore et al. [29,30].

energy, pre-exponential factor and activation enthalpy and Gibbs energy for each reaction (R1–R6) identified in Fig. 3.

The temperature of maximum decomposition rate of each reaction was not significantly affected by the mixing factor as it is shown in Fig. 4a. It is possible to observe in Fig. 4b that the reactions R(1–3), related to hemicelluloses decomposition, showed mean activation energies[1] ranging from 84.69 kJ/mol for R1 in RHW100 to 223.42 kJ/mol for R3 in RHW75. This range of activation energies for hemicellulose decomposition is in agreement with the results reported by Pinzi et al. [33] and Ma et al. [51] through deconvolution of biomass pyrolysis, and by Zhang et al. [52] using isolated hemicellulose. The reactions R1 and R2 were expected to show lower E, since they represent the decomposition of the hemicelluloses present in the husk waste previously treated with citric acid [29]. Nonetheless, the presence of seed waste seems to have produced synergistic effects, since the activation energy of both R1 and R2 in the blends was higher than that for pure RHW. Similarly, R3 presented higher activation energies for RHW50 and RHW75 decomposition than for pure RSW (from which that hemicellulose comes). On the other hand, the activation energy of cellulose decomposition (R4) ranged from 230.11 to 270.85 kJ/mol, being the highest for RHW50. Similar activation energies for cellulose were reported by Zhang et al. [52] for isolated cellulose, and Pinzi et al. [33] through deconvolution procedure. Concerning lignin decomposition (R5), the activation energy was between 187.58 kJ/mol and 303.37 kJ/mol, presenting significant

[1] It should be remembered that isoconversional methods give the result of activation energies for each conversion degree. The mean activation energy, E (calculated from E(α) corresponding to the interval of conversion degrees $0.15 \leq \alpha \leq 0.85$) is informed for all the reactions, although the complete tables are shown in the Supplementary Material, Tables S3–S20.

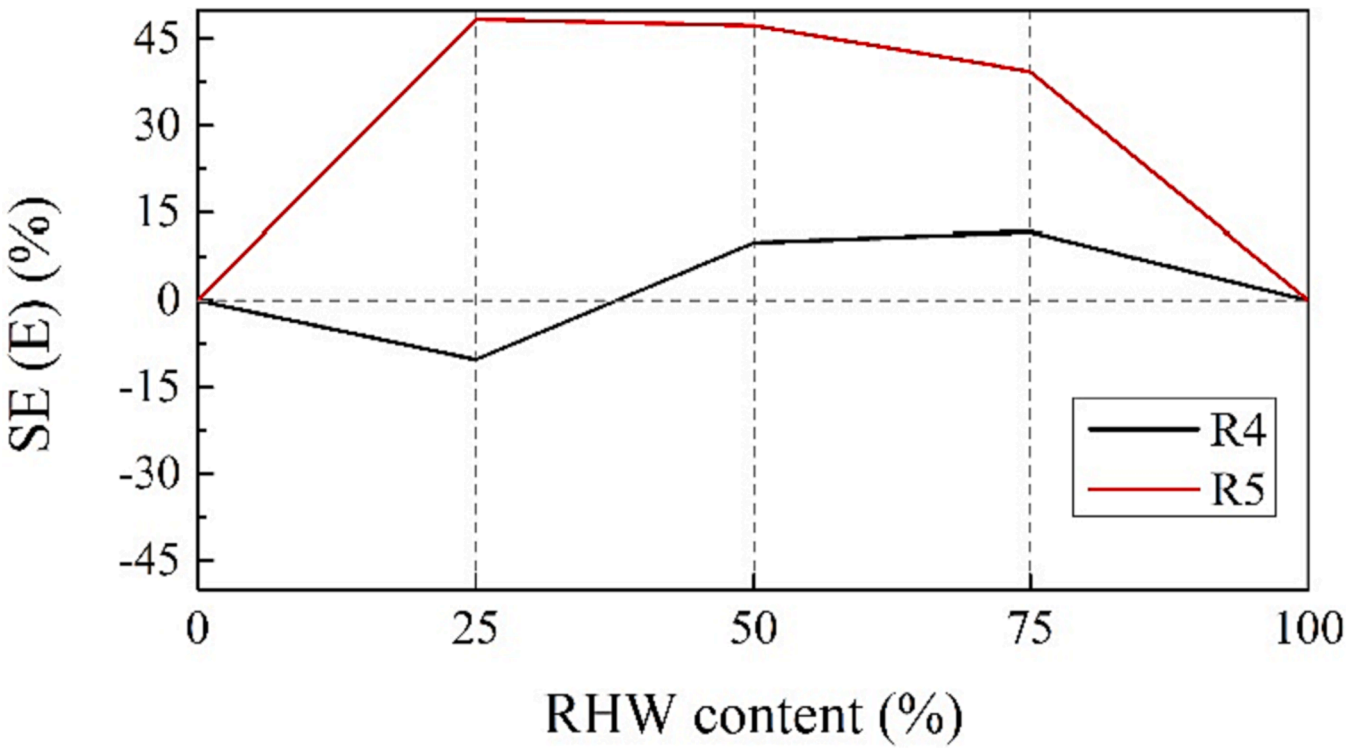

Fig. 5. SE results for the activation energy of the reactions R4 and R5.

synergistic effects, especially for the RHW25 blend. Sharma et al. [53] and Ma et al. [51] found similar activation energies for lignin decomposition in biomass by deconvolution procedure. Overall, the activation energy of the reactions was higher for the blends than for the pure wastes, with the exception of R6. As a consequence of the kinetic compensation effect, the same was observed with the pre-exponential factor, as shown in Fig. 4c. As expected, similar behavior was observed in the ΔH and ΔG (Fig. 4d and e), with higher values for the reactions in the blends, with the exception of R6. The activation enthalpy represents the change in the heat content in the system when bonds are broken in the reagent molecules to form the activated complex [46]. A higher ΔH means that more energy is required to form the activated complex. Therefore, the reactions need more energy in the blends to form the activated complex (except for R6). While cellulose (R4) requires more energy to form the activated complex than lignin (R5) in the pure RSW and RHW, the opposite happens with the blends. ΔG, on the other hand, represents the total energy change in the formation of the activated complex. Since the ΔG of all reactions were positive, it means that they are all non-spontaneous reactions [46].

Since reactions R1, R2, R3 and R6 correspond to decomposition reactions of components that are not presented in both pure wastes, it is not possible to calculate the synergistic effects using Eq. (7)[2]. On the other hand, reactions R4 and R5, corresponding to cellulose and lignin decomposition respectively, appear in both wastes, and the synergistic effect results for E are presented in Fig. 5.

The SE was lower than 15% for the activation energy of R4. While SE was positive for RHW50 and RHW75, it was negative for RHW25. It must be highlighted, that a negative SE is preferable for E, since it means a higher reactivity. On the other hand, the activation energy for lignin decomposition showed a higher positive SE, with values over 45% for RHW25 and RHW50.

Mallick et al. [43] found that the activation energy of the co-pyrolysis of bamboo dust and husk rice was higher than that of the pyrolysis of the pure biomasses. On the other hand, Cheng et al. [54] studied the kinetics of co-pyrolysis of sargassum and poplar, finding that the activation energy was lower than that of the individual pyrolysis of each biomass. According to Salema et al. [42] it is difficult to investigate the exact reasons of the synergistic effects in the activation energy, and that the variations are likely to be produced by changes in the reaction mechanisms and catalytic (or inhibitor) effects.

The conversion functions are presented in Table 1:

In all cases, the n-order function (F_n) was the one that fitted the best as may be observed in Table 1, where $F_n = (1-\alpha)^n$.

The complete results of the activation energy as a function of the conversion degree (Tables S3–S20) and pre-exponential factor (Table S21) determination, together with the master plots (Figs. S6–S23) for the model function for the pyrolysis of the blends are provided in the Supplementary Material.

3.3. Gas, liquid and solid yields

Product yields (by phase) were determined using the vertical reactor described in Section 2.3.3, and are shown in Fig. 6:

The plot shows that synergistic effects are to be considered for all blends, especially concerning gas and biochar yields. Nonetheless, blend

Table 1
Conversion function of the pyrolysis reactions (R1–R6) of RHW0, RHW25, RHW50, RHW75 and RHW100.

f(α)	R1	R2	R3	R4	R5	R6
RHW0[(a)]	–	–	F3	F2.75	F4.8	–
RHW25	F3.3	F0.4	F4.4	F2.2	F5.2	F2.9
RHW50	F3.3	F1.85	F5.2	F2.9	F5	F2.4
RHW75	F3.2	F2.8	F5.5	F3.1	F5	F2.1
RHW100[(b)]	F2.6	F4.7	–	F3.3	F3.9	F2.5

(a) Previously published by Torres-Sciancalepore et al. [30].
(b) Previously published by Torres-Sciancalepore et al. [29].

[2] In the case of these reactions, any change in the kinetic parameters is considered a synergistic effect, since the presence of the other biomass waste is the one producing those changes. Nonetheless, since the components that are decomposing in those reactions are not present in one of the wastes, it becomes impossible to present a numeric value to the synergistic effect.

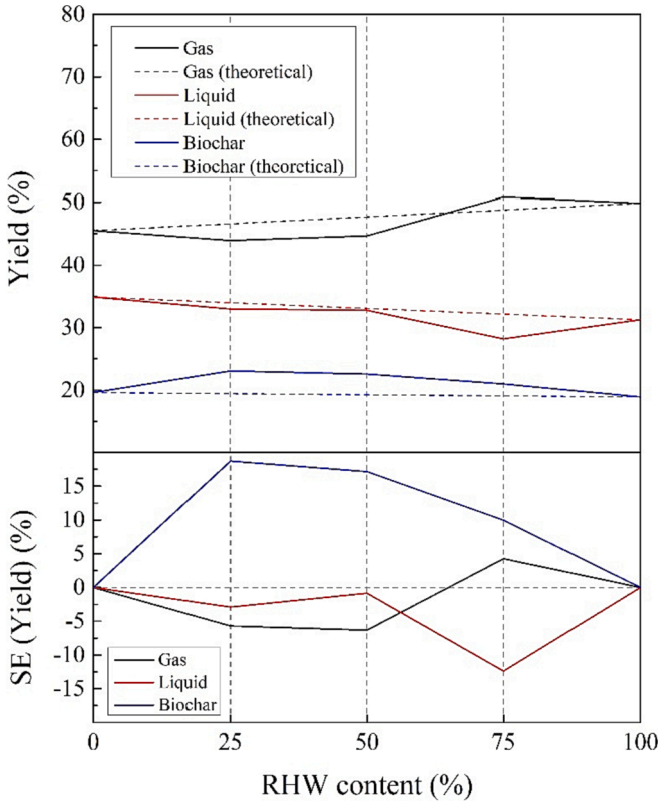

Fig. 6. Gas, liquid and biochar (solid) yields after pyrolysis at 950 °C at a heating rate of 5 °C/min.

RHW75 also shows a significant difference in liquid yield compared to the theoretical value, with the experimental result being 12.4% lower than expected. Blend RHW75 performed best, producing the highest mass of gas with the least tar possible. The positive SE observed for biochar yield is in agreement with the previously presented results of the proximate analysis. Gas yield is similar to that expected according to the model proposed by Torres et al. [55] and Zalazar-García et al. [56], although somewhat lower than reported for pyrolysis of platanus wood by Meng et al. [57].

Wang et al. [58] studied the synergistic effects of co-pyrolysis of *Enteromorpha clathrate* (an algae) and rice husk, finding that the gas yield presented a positive SE (up to 5.90% for the 1:1 blend), while the bio-oil yield showed a negative SE (up to 5.91% for the same blend). According to Wang et al. [58], these SE are explained by an interaction between the biomasses than enhances the secondary cracking reactions of the tar. The biochar yield, however, did not present a significant synergistic effects. Fardi et al. [59] reported the opposite for the co-pyrolysis of potato peel and macroalgae. The gas yield was inhibited by the synergistic effects (SE < 0), while the bio-oil yield was enhanced by the synergistic effects (SE > 0). According to the authors, this was explained by the higher H/C ratio of the potato peel compared to the macroalgae, which produced more H radicals, promoting primary cracking and increasing the volatile yield. It is clear that the interactions between different biomasses may produce different effects. In the case of RHW-RSW blends, the gas and bio-oil yields depend on the mass proportion as well, as may be observed in Fig. 6.

Raza and Abu-Jdayil [60] analyzed the synergistic interactions of date palm seeds and cashew shell waste co-pyrolysis. They found by thermogravimetric analysis that a 1:1 blend produced a higher biochar yield than the pyrolysis of the separate biomasses, similar to what is observed in the RHW-RSW blends.

3.4. Gaseous pyrolysis product analysis

The gases that did not condense inside the horizontal tubular reactor were analyzed by infrared spectroscopy (FTIR) and gas chromatography (GC) with a TCD. Fig. 7a–e shows the absorbance profiles with temperature. The absorbance was read at the wavenumber of the maximum peak for the gas identified. For CO, CO_2, C_2H_4, CH_3OH and CH_4, the absorbance reading was the one corresponding to wavenumbers 2169.5 cm^{-1}, 2360.5 cm^{-1}, 949.75 cm^{-1}, 1033.5 cm^{-1} and 3018.25 cm^{-1}, respectively (an example of FTIR absorbance spectrum is provided in the Supplementary Material, Fig. S24). Since hydrogen gas cannot be detected by FTIR analysis, GC(TCD) was performed and contrasted with an H_2 standard to determine the retention time of the gas in the column. The plot with the H_2 peak area vs. the pyrolysis temperature is shown in Fig. 7f.

Some blends produced more of some gases compared to pure wastes. The production of CO (Fig. 7a) was higher for RHW25 at approximately 350 °C and at 800 °C onwards; while from 400 °C to 700 °C, it showed a local minimum with almost no difference between RHW0, RHW25 and RHW50. In general, RHW100 showed the least production of CO compared to the other samples.

CO_2 release (Fig. 7b) was slightly higher in the blends; RHW25, RHW50 and RHW75 emitted more CO_2 between 200 °C and 400 °C than pure wastes. The synergistic effect became more important from 700 °C onwards, where CO_2 production from RHW25 was noticeably higher than from the other samples.

Ethylene production from the RHW25 blend (Fig. 7c) showed two local maxima at approximately 500 °C and 850 °C, whereas the other samples showed only one maximum at 850 °C and a shoulder at 500–550 °C. At lower temperatures, the highest production of C_2H_4 came from blend RHW25, at temperatures from 550 °C onwards, while the lowest production came from RHW100. On the other hand, blend RHW50 presented the highest production of ethylene at 850 °C with similar absorbance results to pure seed, RHW0.

Methane was the last gas identified by the spectrometer (Fig. 7d), starting at approximately 350 °C. The absorbance maximum was observed at approximately 550 °C for RHW25 and towards higher temperatures (600–700 °C) for the rest of the samples. RHW25 produced the most methane, while RHW100 produced the least.

Maximum methanol was released between 350 °C and 500 °C (Fig. 7e), and was significantly higher for blend RHW25 than for the rest of the samples. This synergistic effect was not very pronounced in the other samples, whose methanol production decreased as RHW was added to the blend.

Gas samples were extracted from the reactor outlet every 10 min (50 °C), and injected into a GC column with TCD to record the area of the peak corresponding to H_2. The plot is shown in Fig. 7f. Hydrogen release occurred in two steps, the first between 200 °C and 400 °C, with very low production compared to the second step, which occurred from 450 °C onwards, with a maximum at approximately 700–750 °C. Fig. 7f

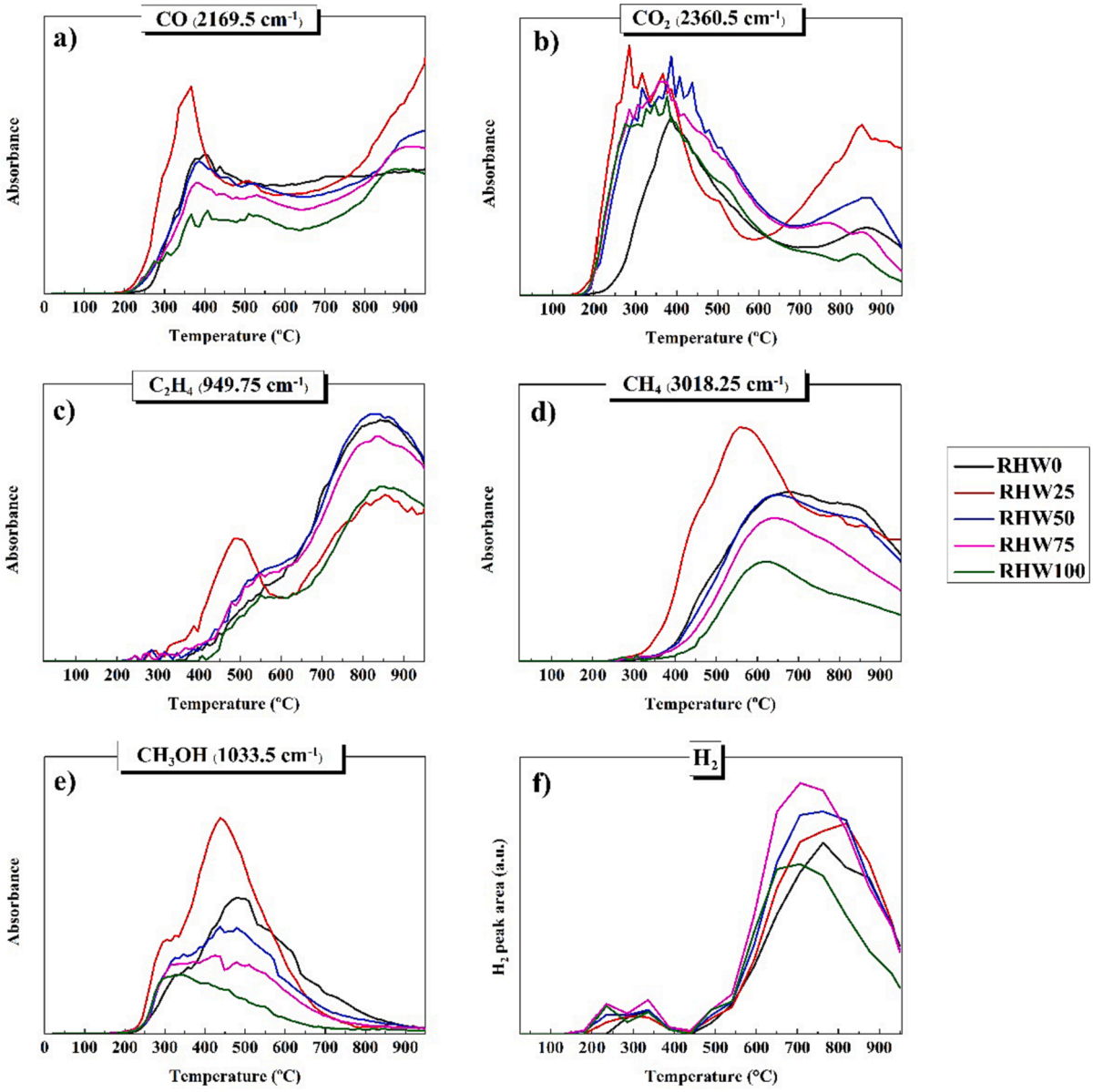

Fig. 7. FTIR Absorbance profiles at characteristic wavenumber for (a) CO, (b) CO_2, (c) C_2H_4, (d) CH_4 and (e) CH_3OH, together with (f) the GC/TCD H_2 peak area profile obtained by pyrolysis of RSW (RHW0), RHW (RHW100) and each blend (RHW25, RHW50, and RHW75).

suggests synergistic effects due to the mixing factor, since all blends produced more hydrogen gas than did the pure wastes. The blend that produced the most H_2 was RHW75, followed by RHW50 and RHW25, successively.

The above analysis is necessary to select the best blend and temperature to obtain the desired gaseous product. For instance, pyrolysis of blend RHW25 at 500 °C releases maximum methanol and methane, while pyrolysis of blend RHW75 at about 750 °C releases maximum hydrogen. Moreover, 750 °C is the temperature at which RHW75 releases maximum ethylene, close to blend RHW50, which had the highest ethylene absorbance. If the desired product is carbon monoxide, the best option is pyrolysis of blend RHW25 at 900 °C.

Table 2 presents the total production of syngas (H_2 and CO) for each sample, expressed in mmol/g of biomass.

Hydrogen production in the current study was similar to those reported by Xu et al. [61] for non-catalytic (blanking) pyrolysis of pure rice husk, and by Blanquet et al. [62] for catalytic pyrolysis of wood pellets at 50 °C/min coupled with non-thermal plasma.

Park et al. [63] studied the co-pyrolysis of food waste and wood bark to produce hydrogen while minimizing pollutant emissions. Pyrolysis experiments were carried out from 300 °C to 700 °C and in all cases, the co-pyrolysis of blends produced higher amounts of hydrogen than the pyrolysis of the biomasses separately. A similar positive SE in H_2 yield was observed by Vuppaladadiyam et al. [64] in the co-pyrolysis of microalgae and swine manure. The authors reported that the carbon monoxide and methane yields were also higher for the blends' co-pyrolysis than the ones from the individual feedstocks' pyrolysis.

Table 2
CO and H_2 production by slow pyrolysis at 950 °C.

	RHW0	RHW25	RHW50	RHW75	RHW100[(a)]
CO (mmol/g biomass)	2.976	3.642	2.978	2.693	2.166
H_2 (mmol/g biomass)	4.079	4.657	5.031	5.639	3.798

[(a)] Previously published by Torres-Sciancalepore et al. [29].

3.5. Condensable pyrolysis product analysis

About 70 different compounds were identified in the tar product through GC–MS. Most of them are phenolic compounds, as shown in Table S22 in the Supplementary Material. The phenolic substances are released as a consequence of lignin cracking. This is because lignin is originally formed by three types of phenylpropane units that are bonded forming very complex structures [50]. Fig. 8 shows the 12 species with the highest peak relative area. Synergistic effects are observed in all samples since the peak area was not as expected for the blends. For instance, diacetone alcohol (2-pentanone, 4-hydroxy-4-methyl-) and mesityl oxide (3-penten-2-one, 4-methyl-) production was significantly

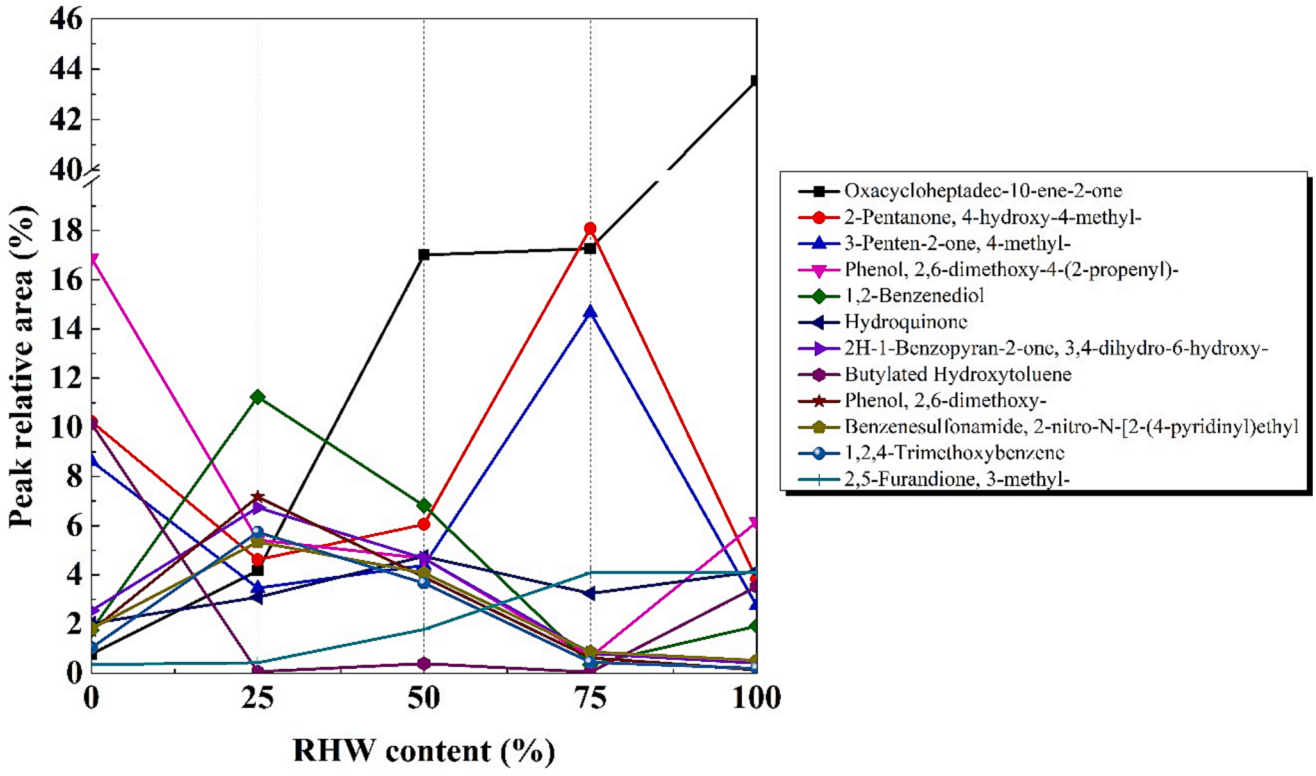

Fig. 8. Twelve main compounds identified by GC–MS in pyrolysis bio-oil (Complete list provided in Table S22, Supplementary Material).

higher for the RHW75 blend. The production of 1,2-benzenediol plus other benzene-derived and phenolic compounds was highest in the RHW25 blend. Butylated hydroxytoluene (BHT) production was inhibited in the blends, with lower production than in the pure wastes. The production of 2,5-furandione, 3-methyl- was higher in the tar of RHW75 pyrolysis. The different substances may be separated by distillation for different uses [29], or burned for energy purposes.

Full chromatograms are provided in the Supplementary Material, Fig. S25.

3.6. Biochar analysis and gasification with CO_2

SEM was used to observe the surfaces of all biochar samples. Three types of solids were identified in the images: seed biochar (Fig. 9), husk biochar (Fig. 10) and filament biochar (Fig. 11). Filaments are hair-like structures found inside the rosehip, which were separated from the seeds and left with the husk.

Figs. 9–11 show that in all biochar particles, the percentage of surface area covered with adhered solids increases with the addition of RHW to the blend. These solids might be inorganic compounds that melted during pyrolysis and resolidified on the surface when the temperature lowered. Proximate analysis showed that the ash percentage increased with the RHW content in the blend, which is consistent with this hypothesis.

As mentioned above, calcium carbonate breaks down at about 700 °C, forming calcium oxide which turns into calcium hydroxide in contact with air humidity. It is thus likely that these solid formations were calcium compounds. Potassium was also present in the ashes, forming $KCaPO_4$ and $K_4Ca(PO_4)_2$ [29]. These depositions in the surfaces of the biochar may be responsible for the synergistic effects discussed in Section 3.1. When these depositions of RHW ashes in the particle surfaces appear in the blends, they affect the release of volatiles as a consequence of the occlusion of pores, leading to lower VM (or higher FC) values than expected by the theoretical calculations. These occlusions may as well be producing the increase in the activation energy of the devolatilization reactions since more energy would be necessary to release the gases and condensable products.

There are micropores in pure RSW biochar, as shown in Fig. 9a. Even

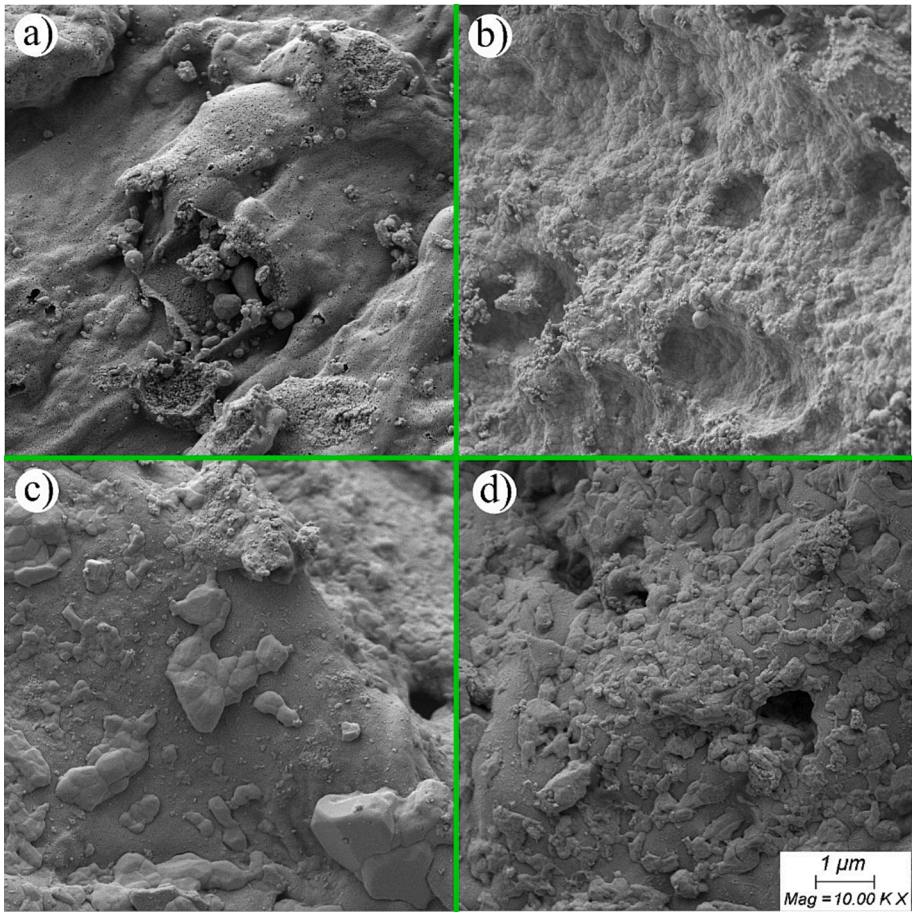

Fig. 9. SEM images (Magnification: 10,000 X) of biochar from seeds in blends: (a) RHW0, (b) RHW25, (c) RHW50 and (d) RHW75.

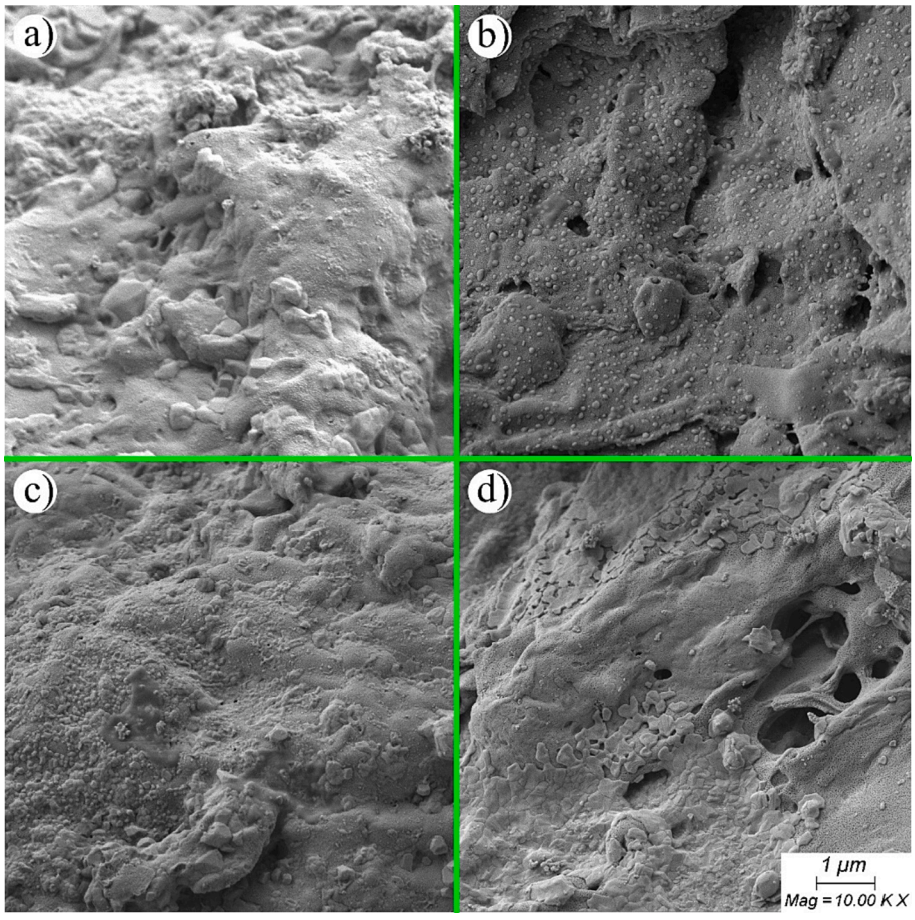

Fig. 10. SEM images (Magnification: 10,000 X) of biochar from husk particles in blends: (a) RHW25, (b) RHW50, (c) RHW75 and (d) RHW100.

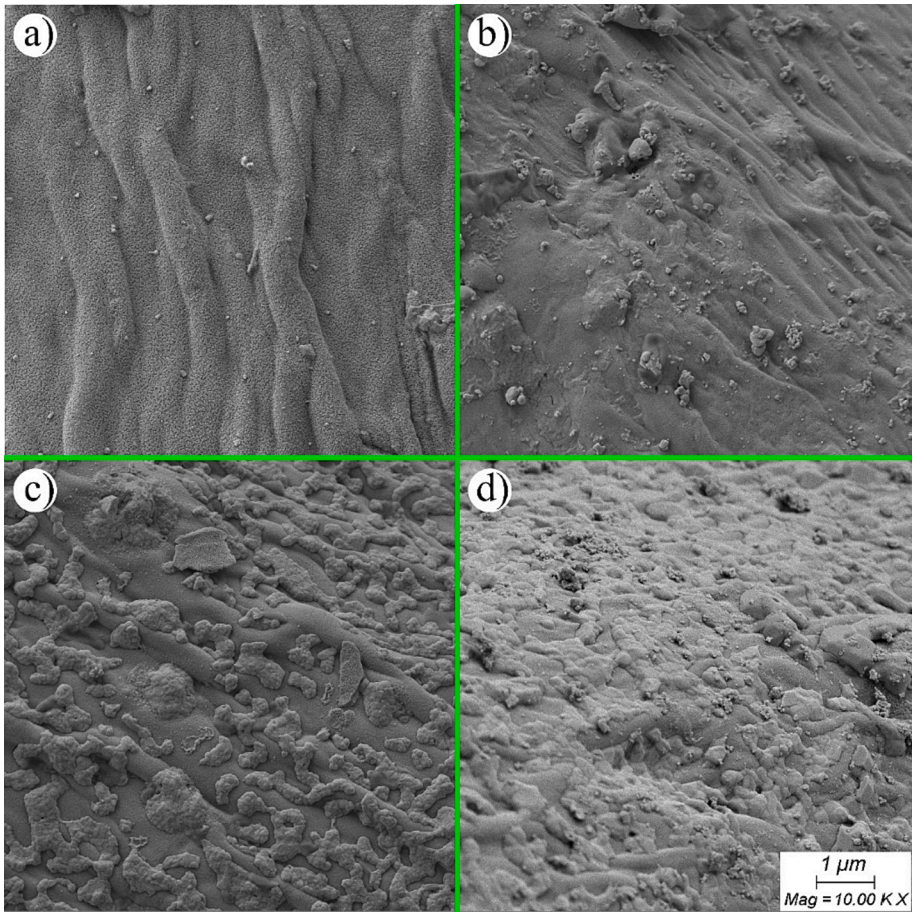

Fig. 11. SEM images (Magnification: 10,000 X) of biochar from filaments in blends: (a) RHW25, (b) RHW50, (c) RHW75 and (d) RHW100.

though some micropores might be occluded by these solids, larger pores are still visible in biochars from blends with a higher percentage of RHW, as shown in Figs. 9d and 10d. In contrast, filament biochar present no pores, but rather folds, as shown in Fig. 11.

To assess the effects of these adhered solids on the biochar surface regarding their reactivity to gasification, experiments with CO_2 were performed. Fig. 12a shows the thermogravimetric results of the gasification reactions. The conversion curves shift to lower temperatures with the addition of RHW, suggesting that biochar reactivity increases with the presence of husk waste in the pyrolysis process by which it was obtained. The reason for the higher reactivity of RHW biochar might be its ash content. The ashes that melted and resolidified on the surface of the biochar particles might have a catalytic effect, thus producing a shift towards lower temperatures for CO_2 gasification. Czerski et al. [65] showed the catalytic effect on CO_2 gasification of tire biochar by adding biomass ash from different sources. In all cases, the presence of biomass ashes produced a shift of the conversion curve towards lower temperatures, showing a catalytic effect [65]. Beech chip ash, as well as RHW, showed over 50% of CaO.

Fig. 12b shows the absorbance spectra obtained by FTIR at a wavenumber of 2169.5 cm^{-1} to identify CO production. These CO absorbance profiles with temperature are in agreement with the conversion plots. No other gas was identified through FTIR (apart from CO and CO_2 which was the gasifying agent). The biochar obtained by pyrolysis is not pure carbon, since it also contains hydrogen and oxygen, though in a much lower proportion. After gasification, the remaining solid is pure ash, meaning that the hydrogen atoms must have left the sample, forming other gases such as H_2, which cannot be detected by FTIR.

To have a qualitative approach about which sample produced the most CO, an integration of the absorbance curves ($\int_{20\,^{\circ}C}^{1050\,^{\circ}C}$ Absorbance dT) in Fig. 12b was made and presented in Table 3.

Table 3 shows that there are synergistic effects in the biochar of all three blends, which all produced more CO than did the pure waste biochars. The biochar from blend RHW50 had the highest CO production.

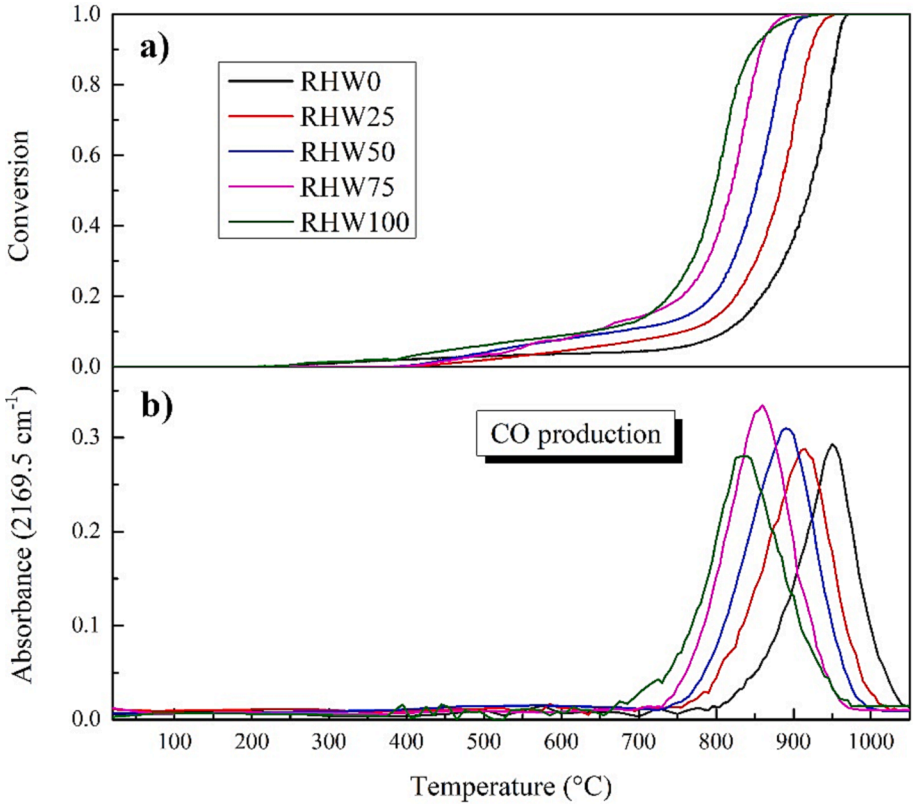

Fig. 12. CO_2 gasification of RHW/RSW biochar (a) conversion with temperature (heating program: 5 °C/min) with (b) FTIR-absorbance at 2169.5 cm^{-1} for CO identification.

Table 3
Cumulative absorbance areas for CO production in the gasification of RHW (0–100) biochar.

	RHW0	RHW25	RHW50	RHW75	RHW100
CO absorbance peak area (a.u.)	34.845	41.119	43.700	42.947	40.953

4. Conclusion

Slow pyrolysis of two *Rosa rubiginosa* rosehip wastes was performed on different blends to study possible synergistic effects. Thermogravimetric analysis was used to determine the kinetic parameters, and it was concluded that there is an overall increase in the activation energy of thermal decomposition in the blends compared to the pure wastes. Synergistic effects were observed in the product yields, since all blends produced more biochar and less bio-oil than expected. Blend RHW75 produced the most gas and the most H_2, while RHW25 produced the most CO and CH_4. Biochar reactivity to gasification was further studied via thermogravimetric and FTIR analyses. Biochar reactivity increased by addition of husk waste to the original biomass blend.

This research demonstrates the potential of valorizing waste from rosehip treatment, and provides valuable information for designing the best conditions according to the desired results, products and their potential applications.

CRediT authorship contribution statement

Rodrigo Torres-Sciancalepore: Writing – original draft, Software, Investigation, Formal analysis, Conceptualization. **Daniela Nassini:** Methodology, Investigation, Formal analysis, Conceptualization. **Daniela Asensio:** Methodology, Investigation, Formal analysis, Conceptualization. **Ana Bohé:** Methodology, Investigation, Funding acquisition, Conceptualization. **Rosa Rodriguez:** Methodology, Investigation, Funding acquisition, Formal analysis, Conceptualization. **Gastón Fouga:** Writing – review & editing, Supervision, Resources, Investigation, Formal analysis, Conceptualization. **Germán Mazza:** Writing – review & editing, Visualization, Supervision, Resources, Project administration, Funding acquisition, Formal analysis.

Declaration of competing interest

The authors declare that they have no known competing financial interests or personal relationships that could have appeared to influence the work reported in this paper.

Data availability

Data will be made available on request.

Acknowledgments

This research was funded by the following Argentine institutions: University of San Juan (PDTS Res. 1054/18); University of Comahue (PIN 2022–04/I260); CONICET -National Scientific and Technical Research Council (PIP 2021–2023 -11220200100950CO); ANPCYT-FONCYT (PICT 2019-01810). Rodrigo Torres-Sciancalepore has a doctoral fellowship from CONICET. Ana Bohé, Rosa Rodriguez, Gastón Fouga and Germán Mazza are Research Members of CONICET, Argentina.

Appendix A. Supplementary material

Supplementary data to this article can be found online at https://doi.org/10.1016/j.enconman.2024.118095.

References

[1] Hura T, Hura K, Svriz M, Rouco C, Ostrowska A, Gadzinowska J, et al. Physiological and molecular features predispose native and invasive populations of sweet briar (Rosa rubiginosa L.) to colonization and restoration of drought degraded environments. Perspect Plant Ecol Evol Syst 2022;56:125690. https://doi.org/10.1016/j.ppees.2022.125690.

[2] Gadzinowska J, Dziurka M, Ostrowska A, Hura K, Hura T. Phytohormone synthesis pathways in sweet briar rose (Rosa rubiginosa L.) seedlings with high adaptation potential to soil drought. Plant Physiol Biochem 2020;154:745–50. https://doi.org/10.1016/j.plaphy.2020.06.018.

[3] Mazzolari AC, Millán EN, Bringa EM, Vázquez DP. Modeling habitat suitability and spread dynamics of two invasive rose species in protected areas of Mendoza, Argentina. Ecol Complex 2020;44:100868. https://doi.org/10.1016/j.ecocom.2020.100868.

[4] Hirsch H, Zimmermann H, Ritz CM, Wissemann V, Wehrden HV, Renison D, et al. Tracking the origin of invasive Rosa rubiginosa populations in Argentina. Int J Plant Sci 2011;172(4):530–40. https://doi.org/10.1086/658924.

[5] Zimmermann H, Ritz CM, Hirsch H, Renison D, Wesche K, Hensen I. Highly reduced genetic diversity of Rosa rubiginosa L. populations in the invasive range. Int J Plant Sci 2010;171:435–46. https://doi.org/10.1086/651244.

[6] Quiroga JM. Análisis preliminar de la cadena de valor de la Rosa Mosqueta en Bariloche y zona de influencia, Argentina. SaberEs 2019;11:65–80.

[7] Franco D, Pinelo M, Sineiro J, Núñez MJ. Processing of Rosa rubiginosa: extraction of oil and antioxidant substances. Bioresour Technol 2007;98:3506–12. https://doi.org/10.1016/j.biortech.2006.11.012.

[8] Eurides D, Antônio L, Daleck R, Maria P, Freitas C. Effect of rose mosqueda extract oil (Rosa aff. Rubiginosa) in cutaneous wound healing. Rev Electrónica Vet 2011;12:1–10.

[9] Nascimento I, Pinheiro Gomes MEPG, Gomes Fernandes NE, Medeiros Azevedo Í, De Alcântara Oliveira Ramalho Borges R, Cunha Medeiros A. Healing of wounds in diabetic rats treated with Rosa rubiginosa oil. J Surg Clin Res 2023;13(2):38–49. https://doi.org/10.20398/jscr.v13i2.31122.

[10] D'Espessailles A, Dossi CG, Espinosa A, González-Mañán D, Tapia GS. Dietary Rosa mosqueta (Rosa rubiginosa) oil prevents high diet-induced hepatic steatosis in mice. Food Funct 2015;6:3109–16. https://doi.org/10.1039/C5FO00741K.

[11] Conteratto C, Artuzo FD, Benedetti Santos OI, Talamini E. Biorefinery: a comprehensive concept for the sociotechnical transition toward bioeconomy. Renew Sustain Energy Rev 2021;151:111527. https://doi.org/10.1016/j.rser.2021.111527.

[12] Mahjoub B, Domscheit E. Chances and challenges of an organic waste–based bioeconomy. Curr Opin Green Sustain Chem 2020;25:100388. https://doi.org/10.1016/j.cogsc.2020.100388.

[13] Bahng MK, Mukarakate C, Robichaud DJ, Nimlos MR. Current technologies for analysis of biomass thermochemical processing: a review. Anal Chim Acta 2009;651:117–38. https://doi.org/10.1016/j.aca.2009.08.016.

[14] Gwenzi W, Chaukura N, Wenga T, Mtisi M. Biochars as media for air pollution control systems: contaminant removal, applications and future research directions. Sci Total Environ 2021;753:142249. https://doi.org/10.1016/j.scitotenv.2020.142249.

[15] Zhao Z, Wang B, Theng BKG, Lee X, Zhang X, Chen M, et al. Removal performance, mechanisms, and influencing factors of biochar for air pollutants: a critical review. Biochar 2022;4:1–24. https://doi.org/10.1007/s42773-022-00156-z.

[16] Wu W, Yang M, Feng Q, McGrouther K, Wang H, Lu H, et al. Chemical characterization of rice straw-derived biochar for soil amendment. Biomass Bioenergy 2012;47:268–76. https://doi.org/10.1016/j.biombioe.2012.09.034.

[17] Yang Z, Fang Z, Zheng L, Cheng W, Tsang PE, Fang J, et al. Remediation of lead contaminated soil by biochar-supported nano-hydroxyapatite. Ecotoxicol Environ Saf 2016;132:224–30. https://doi.org/10.1016/j.ecoenv.2016.06.008.

[18] Mu L, Wang R, Xie P, Li Y, Huang X, Yin H, et al. Comparative investigation on the pyrolysis of crop, woody, and herbaceous biomass: pyrolytic products, structural characteristics, and CO2 gasification. Fuel 2023;335:126940. https://doi.org/10.1016/j.fuel.2022.126940.

[19] Ahmed G, Kishore N. Fuel phase extraction from pyrolytic liquid of Azadirachta indica biomass followed by subsequent characterization of pyrolysis products. Renew Energy 2023;219:119460. https://doi.org/10.1016/j.renene.2023.119460.

[20] Wu Y, Gui Q, Zhang H, Li H, Li B, Liu M, et al. Effect of biomass components' interaction on the pyrolysis reaction kinetics and small-molecule product release characteristics. J Anal Appl Pyrol 2023;173:106039. https://doi.org/10.1016/j.jaap.2023.106039.

[21] Chen WH, Naveen C, Ghodke PK, Sharma AK, Bobde P. Co-pyrolysis of lignocellulosic biomass with other carbonaceous materials: a review on advance technologies, synergistic effect, and future prospectus. Fuel 2023;345:128177. https://doi.org/10.1016/j.fuel.2023.128177.

[22] Li T, Wang J, Chen H, Li W, Pan P, Wu L, et al. Performance analysis of an integrated biomass-to-energy system based on gasification and pyrolysis. Energy Convers Manag 2023;287:117085. https://doi.org/10.1016/j.enconman.2023.117085.

[23] Ayub Y, Zhou J, Shen W, Ren J. Innovative valorization of biomass waste through integration of pyrolysis and gasification: process design, optimization, and multi-scenario sustainability analysis. Energy 2023;282:128417. https://doi.org/10.1016/j.energy.2023.128417.

[24] EL-Sayed SA. Review of thermal decomposition, kinetics parameters and evolved gases during pyrolysis of energetic materials using different techniques. J Anal Appl Pyrol 2022;161:105364. https://doi.org/10.1016/j.jaap.2021.105364.

[25] Vyazovkin S, Burnham AK, Criado JM, Pérez-Maqueda LA, Popescu C, Sbirrazzuoli N. ICTAC Kinetics Committee recommendations for performing kinetic computations on thermal analysis data. Thermochim Acta 2011;520:1–19. https://doi.org/10.1016/j.tca.2011.03.034.

[26] Mishra A, Nanda S, Ranjan Parida M, Jena PK, Dwibedi SK, Manjari Samantaray S, et al. A comparative study on pyrolysis kinetics and thermodynamic parameters of little millet and sunflower stems biomass using thermogravimetric analysis. Bioresour Technol 2023;367:128231. https://doi.org/10.1016/j.biortech.2022.128231.

[27] Sharma A, Aravind Kumar A, Mohanty B, Sawarkar AN. Critical insights into pyrolysis and co-pyrolysis of poplar and eucalyptus wood sawdust: physico-chemical characterization, kinetic triplets, reaction mechanism, and thermodynamic analysis. Renew Energy 2023;210:321–34. https://doi.org/10.1016/j.renene.2023.04.066.

[28] Márquez A, Patlaka E, Sfakiotakis S, Ortiz I, Sánchez-Hervás JM. Pyrolysis of municipal solid waste : a kinetic study through multi-step reaction models. Waste Manag 2023;172:171–81. https://doi.org/10.1016/j.wasman.2023.10.031.

[29] Torres-Sciancalepore R, Riveros-Gomez M, Zalazar-García D, Asensio D, Fabani MP, Rodriguez R, et al. Two-step valorization of invasive species Rosa rubiginosa L. husk waste through eco-friendly optimized pectin extraction and subsequent pyrolysis. J Environ Chem Eng 2023;11(5):110802. https://doi.org/10.1016/j.jece.2023.110802.

[30] Torres-Sciancalepore R, Asensio D, Nassini D, Fernandez A, Rodriguez R, Fouga G, et al. Assessment of the behavior of Rosa rubiginosa seed waste during slow pyrolysis process towards complete recovery: kinetic modeling and product analysis. Energy Convers Manag 2022;272:116340. https://doi.org/10.1016/j.enconman.2022.116340.

[31] Nasrullah A, Khan AS, Khan SZ, Inayat A, Fagieh TM, Bakhsh EM, et al. Kinetics and thermodynamic study of Calligonum polygonoides pyrolysis using model-free methods. Process Saf Environ Prot 2022;160:130–8. https://doi.org/10.1016/j.psep.2022.01.084.

[32] Sun H, Bi H, Jiang C, Ni Z, Tian J, Zhou W, et al. Experimental study of the co-pyrolysis of sewage sludge and wet waste via TG-FTIR-GC and artificial neural network model: synergistic effect, pyrolysis kinetics and gas products. Renew Energy 2022;184:1–14. https://doi.org/10.1016/j.renene.2021.11.049.

[33] Pinzi S, Buratti C, Bartocci P, Marseglia G, Fantozzi F, Barbanera M. A simplified method for kinetic modeling of coffee silver skin pyrolysis by coupling pseudo-components peaks deconvolution analysis and model free-isoconversional methods. Fuel 2020;278:118260. https://doi.org/10.1016/j.fuel.2020.118260.

[34] da Silva JCG, de Albuquerque JG, Galdino WVdA, de Sena RF, Andersen SLF. Single-step and multi-step thermokinetic study – Deconvolution method as a simple pathway for describe properly the biomass pyrolysis for energy conversion. Energy Convers Manag 2020;209:112653. https://doi.org/10.1016/j.enconman.2020.112653.

[35] Liu Y, Song Y, Fu J, Ao W, Ali Siyal A, Zhou C, et al. Co-pyrolysis of sewage sludge and lignocellulosic biomass: synergistic effects on products characteristics and kinetics. Energy Convers Manag 2022;268:116061. https://doi.org/10.1016/j.enconman.2022.116061.

[36] Li W, Huang Y, Liu H, Zhang Y, Jiang Y, Wang Y, et al. Kinetic and thermodynamic studies of biomass pseudo-components under thermo-oxidative degradation conditions using asymmetric function of Bi-Gaussian as deconvolution technique. Renew Energy 2022;188:491–503. https://doi.org/10.1016/j.renene.2022.02.024.

[37] Anyaoha KE. Synergistic perspective on biomass co-utilization in thermo-chemical processes. Bioresour Technol Reports 2022;18:101043. https://doi.org/10.1016/j.biteb.2022.101043.

[38] Dhyani V, Bhaskar T. A comprehensive review on the pyrolysis of lignocellulosic biomass. Renew Energy 2018;129:695–716. https://doi.org/10.1016/j.renene.2017.04.035.

[39] García R, Pizarro C, Lavín AG, Bueno JL. Characterization of Spanish biomass wastes for energy use. Bioresour Technol 2012;103:249–58. https://doi.org/10.1016/j.biortech.2011.10.004.

[40] Zheng NY, Lee M, Lin YL, Samannan B. Microwave-assisted wet co-torrefaction of food sludge and lignocellulose biowaste for biochar production and nutrient recovery. Process Saf Environ Prot 2020;144:273–83. https://doi.org/10.1016/j.psep.2020.07.032.

[41] Kaewpanha M, Guan G, Hao X, Wang Z, Kasai Y, Kusakabe K, et al. Steam co-gasification of brown seaweed and land-based biomass. Fuel Process Technol 2014;120:106–12. https://doi.org/10.1016/j.fuproc.2013.12.013.

[42] Salema AA, Ting RMW, Shang YK. Pyrolysis of blend (oil palm biomass and sawdust) biomass using TG-MS. Bioresour Technol 2019;274:439–46. https://doi.org/10.1016/j.biortech.2018.12.014.

[43] Mallick D, Poddar MK, Mahanta P, Moholkar VS. Discernment of synergism in pyrolysis of biomass blends using thermogravimetric analysis. Bioresour Technol 2018;261:294–305. https://doi.org/10.1016/j.biortech.2018.04.011.

[44] Stefanidis SD, Kalogiannis KG, Iliopoulou EF, Michailof CM, Pilavachi PA, Lappas AA. A study of lignocellulosic biomass pyrolysis via the pyrolysis of cellulose, hemicellulose and lignin. J Anal Appl Pyrol 2014;105:143–50. https://doi.org/10.1016/j.jaap.2013.10.013.

[45] Chen WH, Eng CF, Lin YY, Bach QV. Independent parallel pyrolysis kinetics of cellulose, hemicelluloses and lignin at various heating rates analyzed by evolutionary computation. Energy Convers Manag 2020;221:113165. https://doi.org/10.1016/j.enconman.2020.113165.

[46] Torres-Sciancalepore R, Fernandez A, Asensio D, Riveros M, Fabani MP, Fouga G, et al. Kinetic and thermodynamic comparative study of quince bio-waste slow pyrolysis before and after sustainable recovery of pectin compounds. Energy

Convers Manag 2022;252:115076. https://doi.org/10.1016/j.enconman.2021.115076.
[47] Giudicianni P, Cardone G, Ragucci R. Hemicellulose and lignin slow steam pyrolysis : thermal decomposition of biomass components mixtures. J Anal Appl Pyrol 2013;100:213–22. https://doi.org/10.1016/j.jaap.2012.12.026.
[48] Sanchez-Silva L, López-González D, Villaseñor J, Sánchez P, Valverde JL. Thermogravimetric – mass spectrometric analysis of lignocellulosic and marine biomass pyrolysis. Bioresour Technol 2012;109:163–72. https://doi.org/10.1016/j.biortech.2012.01.001.
[49] Yang H, Yan R, Chen H, Lee DH, Zheng C. Characteristics of hemicellulose, cellulose and lignin pyrolysis. Fuel 2007;86:1781–8. https://doi.org/10.1016/j.fuel.2006.12.013.
[50] Chen D, Cen K, Zhuang X, Gan Z, Zhou J, Zhang Y, et al. Insight into biomass pyrolysis mechanism based on cellulose, hemicellulose, and lignin: evolution of volatiles and kinetics, elucidation of reaction pathways, and characterization of gas, biochar and bio-oil. Combust Flame 2022;242:112142. https://doi.org/10.1016/j.combustflame.2022.112142.
[51] Ma C, Zhang F, Liu H, Wang H, Hu J. Thermogravimetric pyrolysis kinetics study of tobacco stem via multicomponent kinetic modeling, Asym2sig deconvolution and combined kinetics. Bioresour Technol 2022;360:127539. https://doi.org/10.1016/j.biortech.2022.127539.
[52] Zhang J, Chen T, Wu J, Wu J. A novel Gaussian-DAEM-reaction model for the pyrolysis of cellulose, hemicellulose and lignin. RSC Adv 2014;4:17513–20. https://doi.org/10.1039/c4ra01445f.
[53] Sharma P, Pandey OP, Diwan PK. Non-isothermal kinetics of pseudo-components of waste biomass. Fuel 2019;253:1149–61. https://doi.org/10.1016/j.fuel.2019.05.093.
[54] Cheng Z, Gao X, Ma Z, Guo X, Wang J, Luan P, et al. Studies on synergistic effects in co-pyrolysis of sargassum and poplar: thermal behavior and kinetics. J Anal Appl Pyrol 2022;167:105660. https://doi.org/10.1016/j.jaap.2022.105660.
[55] Torres E, Rodriguez-Ortiz LA, Zalazar D, Echegaray M, Rodriguez R, Zhang H, et al. 4-E (environmental, economic, energetic and exergetic) analysis of slow pyrolysis of lignocellulosic waste. Renew Energy 2020;162:296–307. https://doi.org/10.1016/j.renene.2020.07.147.
[56] Zalazar-Garcia D, Fernandez A, Rodriguez-Ortiz L, Rodriguez R, Mazza G. sustainable slow-pyrolysis simulation of 12 lignocellulosic bio-wastes: CO_2 emission, energy, and water consumption. IOP Conf Ser: Earth Environ Sci 2022;952(1):012008. https://doi.org/10.1088/1755-1315/952/1/012008.
[57] Meng H, Wang M, Wu Z, Wang S, Zhao J, Wang Z, et al. Co-pyrolysis of platanus wood and bituminous coal: product distributions, char pore analysis and synergistic effects. J Anal Appl Pyrol 2022;167:105703. https://doi.org/10.1016/j.jaap.2022.105703.
[58] Wang S, Cao B, Feng Y, Sun C, Wang Q, Abomohra A-F, et al. Co-pyrolysis and catalytic co-pyrolysis of Enteromorpha clathrata and rice husk: toward high-quality products. J Therm Anal Calorim 2019;135(4):2613–23. https://doi.org/10.1007/s10973-018-7334-4.
[59] Fardi Z, Shahbeik H, Nosrati M, Motamedian E. Waste-to-energy : co-pyrolysis of potato peel and macroalgae for biofuels and biochemicals. Environ Res 2024;242:117614. https://doi.org/10.1016/j.envres.2023.117614.
[60] Raza M, Abu-Jdayil B. Synergic interactions, kinetic and thermodynamic analyses of date palm seeds and cashew shell waste co-pyrolysis using Coats-Redfern method. Case Stud Therm Eng 2023;47:103118. https://doi.org/10.1016/j.csite.2023.103118.
[61] Xu D, Xiong Y, Zhang S, Su Y. The synergistic mechanism between coke depositions and gas for H2 production from co-pyrolysis of biomass and plastic wastes via char supported catalyst. Waste Manag 2021;121:23–32. https://doi.org/10.1016/j.wasman.2020.11.044.
[62] Blanquet E, Williams PT. Biomass pyrolysis coupled with non-thermal plasma/catalysis for hydrogen production: influence of biomass components and catalyst properties. J Anal Appl Pyrol 2021;159:105325. https://doi.org/10.1016/j.jaap.2021.105325.
[63] Park C, Lee N, Kim J, Lee J. Co-pyrolysis of food waste and wood bark to produce hydrogen with minimizing pollutant emissions. Environ Pollut 2021;270:116045. https://doi.org/10.1016/j.envpol.2020.116045.
[64] Vuppaladadiyam AK, Liu H, Zhao M, Soomro AF, Memon MZ, Dupont V. Thermogravimetric and kinetic analysis to discern synergy during the co-pyrolysis of microalgae and swine manure digestate. Biotechnol Biofuels 2019;12:1–18. https://doi.org/10.1186/s13068-019-1488-6.
[65] Czerski G, Śpiewak K, Grzywacz P, Wierońska-Wiśniewska F. Assessment of the catalytic effect of various biomass ashes on CO2 gasification of tire char. J Energy Inst 2021;99:170–7. https://doi.org/10.1016/j.joei.2021.09.003.